# Second-Harmonic Emission from Quantum Cascade Lasers

**M. Austerer, S. Schartner, M. Nobile, W. Schrenk, A. M. Andrews, T. Roch, G. Strasser**

**Zentrum für Mikro- und Nanostrukturen, TU Wien,
Floragasse 7, A-1040 Vienna, Austria**

## Introduction

The mid-infrared spectral region can be covered by quantum cascade (QC) semiconductor lasers, where the emission wavelength is tailored by bandstructure engineering. For a detailed review on QC lasers see Ref. [1]. Their emission energy is well below the band gaps of the hosting material system. Typical GaAs QC lasers operate in the mid-infrared regime with corresponding energies of ~100 meV, whereas the GaAs band gap is around 1.4 eV. That makes frequency-doubling inside the laser cavity feasible. Such intracavity second-harmonic (SH) generation is not possible in interband semiconductor lasers, where the SH radiation is strongly absorbed. The principle of nonlinear light generation in QC lasers was firstly demonstrated in 2003 [2], since then a lot of progress in this field has been made, such as the improvement of SH generation [3] and the demonstration of third-harmonic generation [4]. A crucial step was the achievement of phase-matching [5], [6], which was demonstrated by means of modal phase-matching in InP-based QC lasers. Another approach for higher conversion efficiencies is quasi phase-matching by periodically modulating the pump current along the QC laser ridge waveguide [7]. Besides up-conversion, other intracavity nonlinear effects are currently being investigated, such as Raman lasing [8] and anti-stokes [9] emission from QC lasers. The above nonlinear effects are due to higher-order susceptibilities of intersubband transitions. Although InP and GaAs, both of which are commonly used as host materials for QC lasers, have nonzero second-order susceptibilities, there is no resulting second-order polarization in the material for QC lasers. That is due to selection rules for intersubband transitions which allow gain only for TM polarized light, which in turn due to crystal symmetry cannot excite nonlinear polarization in the host material. However it was shown that QC lasers grown on ⟨111⟩ substrates, show sum-frequency generation due to bulk nonlinearity [10].

## Bandstructure Engineering and Results

We have investigated second-harmonic and sum-frequency generation in three-well and bound-to-continuum GaAs based QC lasers. The discussed structures are regrowths of structures presented in Ref. [11] and [12] respectively. The second-harmonic generation in these samples is due to intersubband nonlinearities in the active regions of these devices. The optimization of QC active regions for intracavity second-harmonic generation is always jeopardized by the linear absorption that corrupts the laser operation at the fundamental frequency. However, three-well and bound-to-continuum active regions always have higher lying states that can resonantly enhance the second-order susceptibility of the respective QC active region.

The bandstructures discussed in this paper for the GaAs/AlGaAs material system are similar to the structures used for the InGaAs/InAlAs system. However the

GaAs/AlGaAs system offers the advantage of lattice matching for arbitrary $Al_xGa_{1-x}As$ alloy compositions. The highest Γ-valley conduction band offset can thus be reached for AlAs barriers. AlAs barriers have already been used in the past to improve the performance of QC lasers [13] – [15].

Our structure A uses AlAs barriers in the active region to design resonant intersubband transitions to generate frequency doubled light [16]. The Γ-valley conduction band edge of structure A together with the moduli squared of the relevant wavefunctions is shown in Fig. 1. The portion shown is similar to a typical three-well [11] QC active region, but with four AlAs barriers. The AlGaAs barriers in the injector regions have 45% Al-content. The wavefunctions are calculated in an effective mass approximation, where band non-parabolicity is taken into account by an energy-dependent effective mass. The lasing transition between levels 3 and 2 is calculated to an energy of 117 meV with a matrix element of $z_{32}$ = 1.53 nm. Important nonlinear cascades are the level triplets 2–3–5a, 2–3–5b and 2–3–5c. To estimate the second-order susceptibility all three levels (2, 3, 5) have to be considered.

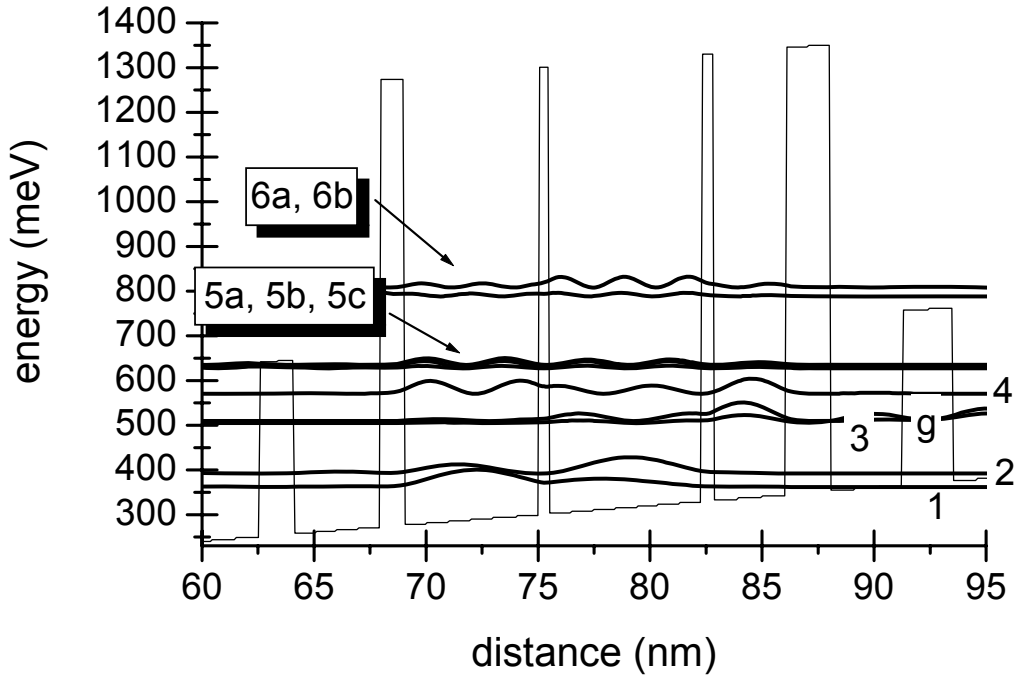


Fig. 1: Conduction band diagram and moduli squared of relevant wavefunctions in the active region of structure A. Important energy levels are labeled “1” through “6” for the active cell and “g” for the injector ground state. The layer thicknesses in nanometers for the GaAs quantum wells and AlAs barriers (italic type) from left to right *1.1*, 6, *0.5*, 6.8, *0.5*, 3.3, *1.9*; The injector bridging regions consist of $GaAs/Al_{0.45}Ga_{0.55}As$ superlattices.

Apart from the QC structure with AlAs barriers in the active region, we also investigated active regions with three-well (structure T) and bound-to-continuum (structure B) active regions, where all the barriers consisted of AlGaAs with 45% Al-content. The band-structures and moduli squared of the wavefunctions for these structures are plotted in Fig. 2. The lasing transition takes place between states 3 and 2. For a detailed description of the laser properties on the fundamental wavelength please refer to references [11] and [12].

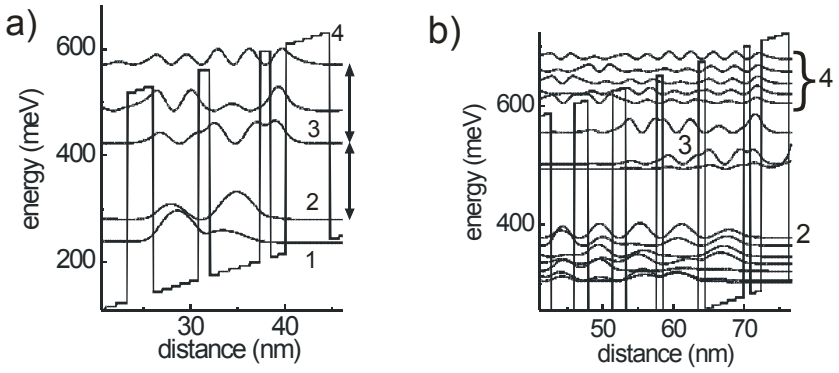


Fig. 2 Portions of the conduction band diagram and the moduli squared wavefunctions of structures a) T and b) B. The most important wavefunctions are labeled 1, 2, 3 and 4. Their functions are described in the text.

So far, SFG was only reported for three-well and two-well design active region QCLs [2], [3], [16]. We demonstrate structure B, where the situation differs qualitatively from these devices. Because the active region of the bound-to-continuum design consists of a superlattice with a thin pre-well, more states significantly contribute to sum-frequency generation. The calculated matrix elements between the involved states (2–4 and 3–4) are in the range of several Å. A feature of this structure, which was already discussed in ref. [12], is the high threshold current density. One reason for this is the strong linear resonant absorption in the active region. In this structure for lower applied fields (<35 kV/cm) the upper states are bound and thus the losses caused by linear absorption are too high to achieve lasing for the fundamental transition 3–2. However, if the electric field is increased these states are shifted towards the border of the barriers, lasing starts and because the states are still close to resonance a high second-order susceptibility is achieved, which leads to efficient sum-frequency generation in these devices.

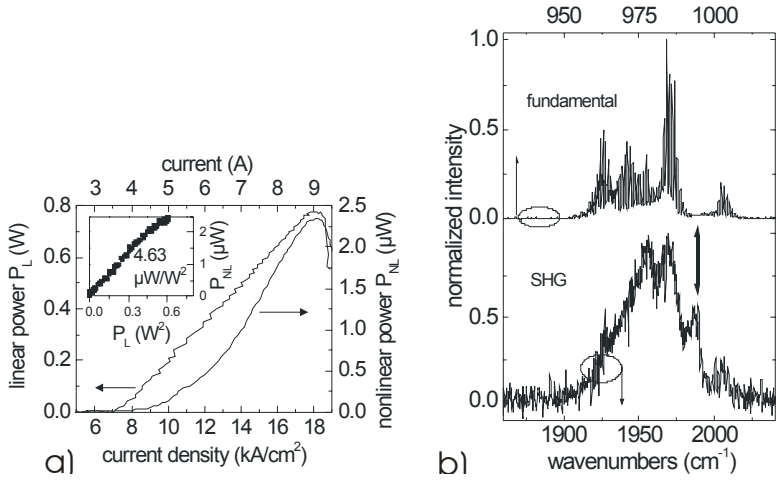


Fig. 3 Light output vs. current characteristics (a) of structure A and the corresponding spectra (b). The sum-frequency signal at 1980 $cm^{-1}$ is indicated by the double-headed arrow.

The fundamental and nonlinear output powers of structure A as a function of drive current are shown in Fig. 3(a). The quadratic dependence of the nonlinear power on the

linear power can be clearly seen. When the nonlinear power is plotted as a function of the fundamental power squared, a linear function is obtained with a slope of ~5 $\mu W/W^2$ (see inset of Fig. 3(a)). In the spectra (Fig. 3(b)) we observe not only the frequency-doubled signal, but also a sum-frequency signal at ~1980 $cm^{-1}$, which arises from the two distinct Fabry-Perot combs at 980 $cm^{-1}$ and 1000 $cm^{-1}$.

The bound-to-continuum active region shows the best conversion efficiency, possibly due to the multitude of upper states in the nonlinear cascade. Both the three-well designs with AlGaAs and AlAs barriers show approximately the same conversion efficiency, so there is no significant advantage with the additional barrier height provided by the AlAs material.

## References

[1] C. Gmachl, F. Capasso, D. L. Sivco, and A. Y.Cho, Rep. Prog. Phys. 64, 1533 (2001)

[2] N. Owschimikow, C. Gmachl, A. Belyanin, V. Kocharovsky, D. L. Sivco, R. Colombelli, F. Capasso, and A. Y. Cho, Phys. Rev. Lett. 90, 043902 (2003)

[3] C. Gmachl, A. Belyanin, D. L. Sivco, M. L. Peabody, N. Owschimikow, A. M. Sergent, F. Capasso, and A. Y. Cho, IEEE J. Quantum Electron. 39, 1345 (2003)

[4] T. S. Mosely, A. Belyanin, C. Gmachl, D. L. Sivco, M. L. Peabody, and A.Y Cho, Opt. Express 12, 2976 (2004)

[5] O. Malis, A. Belyanin, D. L.Sivco, M. L. Peabody, A. M. Sergent and A. Y. Cho, Appl. Phys. Lett. 84, 2721 (2004)

[6] O. Malis, A. Belyanin, D. L. Sivco, J. Chen, A.M. Sergent, C. Gmachl and A. Y. Cho, Electron. Lett. 40, 1586 (2004)

[7] M. A. Belkin, M. Troccoli, L. Diehl, F. Capasso, A. Belyanin, and D. L. Sivco, in Conference on Lasers and Electro-Optics/Quantum Electronics (Optical Society of America, Washington, DC, 2005), QPDA1

[8] M. Troccoli, A. Belyanin, F. Capasso, E. Cubukcu, D. L. Sivco and A.Y. Cho, Nature 433, 845 (2005)

[9] H. Page, C. Becker, A. Robertson, G. Glastre, V. Ortiz, and C. Sirtori, Appl. Phys. Lett. 78, 3529 (2001)

[10] J.-Y. Bengloan, A. DeRossi, V. Ortiz, X. Marcadet, M. Calligaro, I. Maurin, and C. Sirtori, Appl. Phys. Lett. 84, 2019 (2004)

[11] H. Page, C. Becker, A. Robertson, G. Glastre, V. Ortiz, and C. Sirtori, Appl. Phys. Lett. 78, 3529 (2001)

[12] C. Pflügl, W. Schrenk, S. Anders, G. Strasser, C. Becker, C. Sirtori, Y. Bonetti, and A. Muller, Appl. Phys. Lett. 83, 4698 (2003)

[13] L. R. Wilson, D. A.Carder, J. W. Cockburn, R. P. Green, D. G. Revin, M. J. Steer, M. Hopkinson, G. Hill, and R. Airey, Appl. Phys. Lett. 81, 1378 (2002)

[14] M. P. Semtsiv, M. Ziegler, S. Dressler, T.W. Masselink, N. Georgiev, T. Dekorsky, and M. Helm, Appl. Phys. Lett. 85, 1478 (2004)

[15] W. Schrenk, N. Finger, S. Gianordoli, E. Gornik, and G. Strasser, Appl. Phys. Lett. 77, 3328 (2000)

[16] C. Pflügl, M. Austerer, W. Schrenk, and G. Strasser, Electron. Lett. 41, 1331 (2005)